Two modes of change in Southern Ocean productivity over the past million years

Jaccard, S.L.[1], Hayes, C.T.[2], Martinez-Garcia, A.[1], Hodell, D.A.[3], Anderson, R.F.[2], Sigman, D.M.[4], Haug, G.H.[1]

[1] Geological Institute, Department of Earth Sciences, ETH Zürich, Switzerland
[2] Lamont-Doherty Earth Observatory, Columbia University, Palisades, New York, USA.
[3] Godwin Laboratory for Paleoclimate Research, Department of Earth Sciences, University of Cambridge, Cambridge, UK.
[4] Department of Geosciences, Princeton University, Princeton, USA.

Export of organic carbon from surface waters of the Antarctic zone of the Southern Ocean decreased during the last ice age, coinciding with declining atmospheric CO_2 concentrations, signaling reduced exchange of CO_2 between the ocean interior and the atmosphere. In contrast, in the Subantarctic Zone, export production increased into ice ages coinciding with rising dust fluxes and thus suggesting iron fertilization of Subantarctic phytoplankton. Here, a new high-resolution productivity record from the Antarctic zone is compiled with parallel Subantarctic data over the last million years. Together, they fit the view that the combination of these two modes of Southern Ocean change determines the temporal structure of the glacial/interglacial atmospheric CO_2 record, including during the interval of "lukewarm" interglacials between 450 and 800 thousand years ago.

Antarctic ice core measurements reveal that regional air temperatures and atmospheric pCO_2 were tightly correlated over glacial-interglacial cycles of the past 800 kyrs (*1*). Many studies have inferred a dominant role for the Southern Ocean in modulating glacial-interglacial variability of atmospheric pCO_2 ((*2*) and references therein). The central role of the Southern Ocean is thought to reflect its leverage on the global efficiency of the biological pump, in which the production, sinking, and deep remineralization of organic matter sequesters carbon in the ocean interior, lowering atmospheric CO_2. Dense subsurface water masses outcrop in the Southern Ocean, providing exchange pathways between the deep ocean and the atmosphere. Vertical exchange of water causes deeply sequestered CO_2 and nutrients to be mixed to the surface, fueling high rates of phytoplankton productivity. Today, the Southern Ocean is the principal leak in the biological pump, because export production is inadequate to prevent the evasion of deeply sequestered carbon when waters are exposed to the atmosphere. The polar CO_2 leak can be directly inhibited during glacial stages by factors such as increased sea-ice cover (*3*) and/or changes in buoyancy forcing and convection (*4, 5*). In addition, the glacial CO_2 reduction associated with these mechanisms would have been amplified by iron fertilization of the Subantarctic Zone (SAZ) of the Southern Ocean (*6, 7*) and associated alkalinity feedbacks (*8*).

Export production records from the Antarctic Zone (AZ) have been used to trace changes in the rate of Southern Ocean overturning through time (*9, 10*). However, these records only cover the last glacial cycle, restricting our understanding of the evolution of the Antarctic component of this two-mode system by which the Southern Ocean regulates the transfer of carbon between the ocean interior and the atmosphere over previous climatic cycles. Here, we report a high-resolution relative elemental concentration record from Ocean Drilling Program (ODP) site 1094 (53.2°S, 05.1°E; water depth 2,850 m) (Fig. 1), which traces changes in AZ export production over the past million years (SOM, Figs S1 & S2). The time resolution achieved here rivals the measurement density typical for Antarctic ice-core records. These observations are complemented with reconstruction of ^{230}Th-normalized biogenic particle flux to the seafloor covering the last two glacial terminations (Fig. 2).

The pelagic sediment analyzed in this study is dominantly composed of diatomaceous opal and terrigenous detritus, the latter of which is mostly ice-rafted, with a minor contribution from aeolian material (*11*). Assuming that sedimentary iron (Fe) is of detrital origin, barium (Ba) abundance normalized to Fe yields an estimate of the sedimentary concentration of biogenic (or excess) Ba (bioBa), which serves as a tool to reconstruct changes in the integrated flux of organic matter to the sediment (*12*). Normalization by Fe assumes that the detrital fraction has not varied significantly in space and time, supported by provenance studies, indicating that the tephra-rich terrigenous material at this site is consistently derived from the South Sandwich volcanic arc, with negligible contribution from Bouvet Island and possibly the Antarctic Peninsula (*11*). Calcium (Ca) normalized to Fe indicates the sedimentary concentration of biogenic carbonate ($CaCO_3$). The records of Fe and Ti show almost identical trends in amplitude, but XRF signals are better for Fe, which is thus used for normalization. In these opal-rich sediments, elemental spectrum processing does not allow proper quantification of Al because of the overlapping Si peaks, precluding the use of Al as a normalizing agent.

The Ba/Fe record shows a strong climate-related signal (Fig. 3C), with high values during interglacials and lower values during cold stages. The Ba/Fe record is in good agreement with the ^{230}Th-normalized flux of bioBa (Fig. 2C), supporting the use of Ba/Fe to infer bioBa throughout the record. The large-scale Ba variations cannot be explained as the result of bacterially-mediated sulfate reduction and associated diagenetic barite ($BaSO_4$) dissolution because no significant sulfate reduction is observed in the interstitial water of Pleistocene sediments of ODP site 1094 (*13*). Indeed, the ^{230}Th-normalized flux of bioBa is similar to that of opal and chlorophyll transformation products (chlorins) measured in the same sediment core (Fig. 2). Preservation of these independent paleo-productivity proxies is favored in different sedimentary environments. While the preservation of bioBa can be compromised by reducing conditions, the preservation of organic matter in general, and chlorins in particular, is enhanced when oxygen content is low (*14*). The preservation of opal is unrelated to the redox state of sediments but primarily driven by the total sedimentation rate (*15*). The correlation between opal fluxes and excess ^{231}Pa/^{230}Th at the same core site during the last 25 kyrs (*9*) and the correlation between opal fluxes and bioBa over the last 150 kyrs reported here indicate that the reconstructed opal fluxes most likely represent variable production by diatoms.

Consequently, the sedimentary Ba/Fe is interpreted to indicate lower bioBa accumulation and thus less export of organic matter from the surface ocean during cold periods, with the lowest bioBa concentrations coinciding almost exclusively with the glacial maxima, consistent with measurements elsewhere in the Southern Ocean, south of the polar frontal zone ((*16*) and references therein) (Fig. S3). Sea-ice has the potential to directly alter export production, by blocking sunlight vital for phytoplankton to undertake photosynthesis; however, sea-ice was only present at this site during the winters of glacial periods (*17*), not during the summer growing season. Rather, changes in export imply a reduced supply of nutrients to the surface ocean. Phytoplankton growth is inhibited by the lack of bioavailable Fe in most parts of the Southern Ocean. Vertical mixing and upwelling (rather than atmospheric fluxes) appear to dominate the supply of Fe to the Antarctic surface ocean at present (*18*). Thus, glacial decrease in productivity may have been driven by a reduction in this deep water-derived iron supply.

While various physical mechanisms have been proposed for a reduction in this deep water exposure, they all involve reduction of wind-driven upwelling, wintertime vertical mixing, or both (*4, 5, 19*). Upwelling could be lowered by weaker westerlies and/or by a more northerly position for them, while wintertime vertical mixing is sensitive to upper ocean density stratification. Various processes can affect this stratification, including upwelling, which strips away the freshwater cap (halocline) that maintains vertical stability.

Of the nitrate imported into the Antarctic surface today, only a portion derives from Ekman upwelling, with the remaining deriving from wintertime vertical mixing (*20*). Given that the data suggest many fold lower export production during peak ice ages, we infer that these changes in productivity likely require both a reduction in wind-driven upwelling and an increase in density stratification. This is significant in that the latter change would affect deep water formation, through which the Antarctic has its greatest direct leverage on atmospheric CO_2 (*21, 22*).

Upon glacial terminations, large pulses of export production coincide with prominent increases in atmospheric CO_2 concentrations reconstructed from Antarctic ice cores (Figs. 2 & 3). Flux determinations of three independent export production proxies suggest that the export of organic matter increased by more than an order of magnitude across the two last climate transitions (Fig. 2). Reconstruction of past silicon and nitrogen dynamics suggest that relative nutrient utilization did not rise sharply at the last glacial termination (*23*), such that the rise in Ba and opal flux was a response to a large increase in the nutrient supply to the euphotic zone. These increases in export were accompanied by summer sea-surface temperature (SST) overshoots and abrupt disappearances of winter sea-ice (*17*). Summer SSTs increased by more than 4°C in less than 5 kyrs for the last five glacial terminations (*17*). While the sequence of deglacial events remains to be resolved (*9*), the systematic and repeated glacial-to-interglacial rises in biogenic flux (Fig. 3) point to a robust pattern of enhanced Southern Ocean overturning during interglacials.

Moreover, we show that these glacial-to-interglacial export production increases were accompanied by short-lived $CaCO_3$ spikes in these otherwise carbonate-poor sediments (Fig. 3D). We note that the preservation spike observed for the last glacial termination is muted at this site, for reasons that remain unclear. The near-absence of $CaCO_3$ in most of the record suggests that seafloor preservation of the $CaCO_3$ rain regulated the bimodal character of the record. Although intervals with higher sedimentary $CaCO_3$ concentrations could in principle reflect increased local $CaCO_3$ export, the abrupt increases and the transient nature of the $CaCO_3$ spikes compared to export production proxies argue instead for a deepening of the lysocline, as expected if CO_2 was lost from deep waters at this time.

The decrease in deep water exposure following peak interglacial conditions, indicated by declining export production, leads to CO_2 reduction, and this mechanism appears to apply in particular to the early stages of glaciation. As a general rule, elevated Antarctic export occurs during the peak interglacials, giving way to a major decline in the early stages of glaciation (Fig. 3 C), coinciding with the first half of the CO_2 decline into each glacial period, 40-50 ppm (Fig. 3A, reaching ~225 ppm). Remarkably, this is a similar, if slightly greater, reduction to the estimate from numerical models for the CO_2 decline that should result from a strong reduction in Antarctic overturning (Brovkin et al., 2007; Hain et al., 2011). While further declines in Antarctic export production occur later in the glacial progression (Fig. 3C), the associated CO_2 reduction associated with this mechanism should have nearly saturated (*2*). However, based on data from ODP Site 1090 in the Subantarctic Zone (SAZ) to the north of ODP Site 1094, it appears that the later stages of glaciation and climate cross a threshold at which the SAZ undergoes a dramatic rise in productivity (Fig. 3F) (*6, 24*) coincident with increased dust-borne iron supply to the SAZ from continental regions upstream in the westerly wind field (Fig. 3E; (*7*)). Iron fertilization in the SAZ would have permitted biological productivity in this region to sequester additional regenerated carbon in the abyssal ocean, which would have further lowered atmospheric CO_2 (*16, 25*). It is again notable that numerical model simulations of Subantarctic iron fertilization predict roughly the observed CO_2 declines of ~ 40 ppm that occur later in the glacial progressions (*21, 25, 26*). In the modern ocean, there is upper ocean mixing across the fronts separating the AZ and SAZ (*27*). Thus, during peak ice conditions, iron fertilization in the SAZ may have further depleted the AZ of surface nutrients, contributing to the continued decline of AZ export production to its glacial minimum. In any case, it is a remarkable characteristic of the two records that the SAZ biological response begins when AZ productivity has reached the lower half of its range (Fig. 3C and F), with relatively little correlated variation between the AZ and SAZ (Fig. 4), and that the major changes in each correspond to roughly half of the observed CO_2 variation (Fig. 4). In summary, the paleoceanographic records from both the AZ and SAZ merge with the numerical model estimates of Southern Ocean to provide a coherent two-part Southern Ocean mechanism for the amplitude and timing of glacial interglacial CO_2 change.

The potential for these two modes of the Southern Ocean to have different roles in glacial/interglacial CO_2 change, first recognized in the context of the last glacial cycle (*2, 16*), is bolstered by the data reported here for the period of the "lukewarm" interglacials (MIS 13-19). The lukewarm interglacials are characterized by reduced amplitude of the ice-core δD and CO_2 records (Fig. 3) and a general decrease in global interglacial temperatures that appears to be more pronounced in Southern Ocean SST records (*28*). Given the potential dependencies of westerly wind position (*29*) and polar ocean water-column stability (*30*) on global temperature, the muting of the pCO_2 increase during the lukewarm interglacials might have been linked to a reduced dynamic range of Antarctic overturning, with the abyssal ocean thereby maintaining a larger reservoir of regenerated carbon than in more recent interglacials (*31*). This hypothesis is supported by the Antarctic Ba/Fe record (Fig. 3C), which shows markedly reduced amplitude for the Ba/Fe maxima associated with the lukewarm interglacials (Fig. 4, squares with open circles along the x axis). Furthermore, this interval also generally has reduced deglacial $CaCO_3$ peaks (Fig. 3D), which would suggest that proportionally less CO_2 was released from the deep ocean. The expression of interglacials in the SAZ record is indistinguishable between the period containing the lukewarm interglacials and the rest of the record (Figs. 3 & 4) (*7, 24*), suggesting that the cessation of SAZ iron fertilization occurred during the lukewarms as in other interglacials.

In contrast to the lukewarm interglacials, MIS 21 and 25 were characterized by full-amplitude export production peaks in the AZ accompanied by large $CaCO_3$ preservation events, suggesting an increase in upwelling and deep-ocean CO_2 release during Terminations X and XI (Fig. 3), consistent with planktic foraminiferal pH estimates that suggest that both interglacials had pCO_2 values as high as recent interglacials (*32*). This observation further argues that the subsequent lukewarm interglacials represented a distinct period. Our observations thus indicate a strong coupling between Antarctic deep-to-surface exchange and the magnitude of the CO_2 release from the ocean interior, which is consistent with observed changes in atmospheric pCO_2 even beyond the interval covered by the Antarctic ice-core records.

There is much uncertainty and debate regarding the response of Southern Ocean overturning to ongoing global warming, as well to its impact on the oceanic uptake of anthropogenic CO_2 (*33*). The paleoclimate data reported here argue strongly for a robust sensitivity of Antarctic overturning to global climate, in which overturning increases under warmer conditions. As the physical mechanism of this coupling is not yet clear, one cannot be confident that it will apply on the decadal to centennial scale and under the specific conditions of anthropogenic global warming. Nonetheless, the finding of stronger overturning under warmer climates, taken at face value, suggests a similar sense of change in the warmer future ocean.

Figure captions

Fig. 1 Core locations represented on the January-March sea-surface temperature field. The black line delineates maximum winter sea-ice extent (using the 90% winter sea-ice concentration line) based on the Hadley Center sea-ice concentration data 1978-2010 (*34*).

Fig. 2 Biogenic particle flux reconstructed by ^{230}Th-normalization for four independent proxies covering the last two glacial terminations. Discrete measurements for the upper 25 kyrs have been performed on TN-57-13PC. (A) atmospheric pCO_2 (*1, 35*); (B) comparison between $CaCO_3$ flux and Ca/Fe; (C) comparison between bioBa flux and Ba/Fe; (D) chlorin flux; (E) biogenic opal flux. Blue shadings highlight ice ages, whereas red shadings indicate interglacials. The two arrows highlight the two step-transition into ice ages.

Fig. 3 Records of (A) atmospheric pCO_2 (*1*), (B) ODP 1094 planktic foraminifera $\delta^{18}O$ (*36, 37*), (C) ODP 1094 Ba/Fe (data smoothed by a five-point running mean), (D) ODP 1094 Ca/Fe (data smoothed by a five-point running mean), (E) Fe flux to subantarctic core ODP1090 (*7*), and (F) ODP 1090 sedimentary alkenone concentration (*24*) covering the past 1 Myr. Red/grey shadings highlight intervals were Antarctic (AZ)/subantarctic (SAZ) processes, respectively, are dominantly controlling the partitioning of CO_2 between the ocean interior and the atmosphere.

Fig. 4 Comparison between ODP 1094 Ba/Fe and ODP 1090 sedimentary alkenone concentration (*24*). Symbol colour indicates pCO_2. Filled circles illustrate the period 0-450 kyrs, filled squares the lukewarm interval (450-800 kyrs) and the open squares the interval 800-1000 kyrs for which pCO_2 reconstruction do not yet exist.

References and Notes

References

1. D. Lüthi *et al.*, High-resolution carbon dioxide concentration record 650,000-800,000 year before present. *Nature* **453**, 379 (2008).
2. D. M. Sigman, M. P. Hain, G. H. Haug, The polar ocean and glacial cycles in atmospheric CO_2 concentration. *Nature* **466**, 47 (2010).
3. R. F. Keeling, B. B. Stephens, Antarctic sea ice and the control of Pleistocene climate instability. *Paleoceanography* **16**, 112 (2001).
4. J J. R. Toggweiler, J. L. Russell, S. Carson, Midlatitude westerlies, atmospheric CO_2 and climate change during ice ages. *Paleoceanography* **21**, PA2005 (2006).
5. A. J. Watson, A. C. Naveira Garabato, The role of Southern Ocean mixing and upwelling in glacial-interglacial atmospheric CO_2 change. *Tellus* **58B**, 73 (2006).
6. N. Kumar *et al.*, Increased biological productivity and export production in the glacial Southern Ocean. *Nature* **378**, 675 (1995).
7. A. Martinez-Garcia *et al.*, Southern Ocean dust–climate coupling over the past four million years. *Nature* **476**, 312 (2011).
8. R. Keir, On the late Pleistocene ocean geochemistry and circulation. *Paleoceanography* **3**, 413 (1988).
9. R. F. Anderson *et al.*, Wind-Driven Upwelling in the Southern Ocean and the Deglacial Rise in Atmospheric CO_2. *Science* **323**, 1143 (2009).
10. R. François *et al.*, Contribution of Southern Ocean surface-water stratification to low atmospheric CO_2 concentrations during the last glacial period. *Nature* **389**, 929 (October 30, 1997, 1997).
11. S. H. H. Nielsen, D. A. Hodell, G. Kamenov, T. Guilderson, M. R. Perfit, Origin and significance of ice-rafted detritus in the Atlantic sector of the Southern Ocean. *Geochemistry, Geophysics, Geosystems* **8**, Q12005 (2007).
12. J. Dymond, E. Suess, M. Lyle, Barium in deep-sea sediments: A geochemical proxy for paleoproductivity. *Paleoceanography* **7**, 163 (1992).
13. R. Gersonde, D. A. Hodell, P. Blum, in *Proceedings of the Ocean Drilling Program, Initial Results* (Ocean Drilling Program, College Station, TX, 1999), vol. 177, pp. 1-67.
14. K. A. F. Zonneveld *et al.*, Selective preservation of organic matter in marine evironments; processes and impact on the sedimentary record. *Biogeosciences* **7**, 483 (2010).
15. F. L. Sayles, W. R. Martin, Z. Chase, R. F. Anderson, Benthic remineralization and burial of biogenic SiO_2, $CaCO_3$, organic carbon, and detrital material in the Southern Ocean along a transect at 170° West. *Deep-Sea Research II* **48**, 4323 (2001).
16. K. Kohfeld, C. Le Quéré, S. P. Harrison, R. F. Anderson, Role of Marine Biology in Glacial-Interglacial CO_2 Cycles. *Science* **308**, 74 (2005).
17. A. Schneider-Mor *et al.*, Diatom stable isotopes, sea ice presence and sea surface temperature records of the past 640 ka in the Atlantic sector of the Southern Ocean. *Geophysical Research Letters* **32**, L10704 (2005).

18. N. Lefèvre, A. J. Watson, Modeling the geochemical cycle of iron in the oceans and its impact on atmospheric CO_2 concentrations. *Global Biogeochemical Cycles* **13**, 727 (1999).
19. A. E. S. Kemp, I. Grigorov, R. B. Pearce, A. C. Naveira Garabato, Migration of the Antarctic Polar Front through the mid-Pleistocene transition: evidence and climatic implications. *Quaternary Science Reviews* **29**, 1993 (2010).
20. M. J. Lourey, T. W. Trull, Seasonal nutrient depletion and carbon export in the Subantarctic and Polar Frontal Zones of the Southern Ocean south of Australia. *Journal of Geophysical Research* **106**, 31 (2001).
21. M. P. Hain, D. M. Sigman, G. H. Haug, Carbon dioxide effects of Antarctic stratification, North Atlantic Intermediate Water formation, and subantarctic nutrient drawdown during the last ice age: Diagnosis and synthesis in a geochemical box model. *Global Biogeochemical Cycles* **24**, GB4023 (2010).
22. I. Marinov, A. Gnanadesikan, J. L. Sarmiento, J. R. Toggweiler, B. K. Mignone, Impact of oceanic circulation on biological carbon storage in the ocean and atmospheric $p\mathrm{CO}_2$. *Global Biogeochemical Cycles* **22**, GB3007 (2008).
23. M. G. Horn, C. P. Beucher, R. S. Robinson, M. A. Brzezinski, Southern Ocean nitrogen and silicon dynamics during the last glacial termination. *Earth and Planetary Science Letters* **311**, 334 (2011).
24. A. Martinez-Garcia *et al.*, Links between iron supply, marine productivity, sea surface temperature, and CO_2 over the past 1.1 Ma. *Paleoceanography* **24**, PA1207 (2009).
25. A. J. Watson, D. C. E. Bakker, A. J. Ridgwell, P. W. Boyd, C. S. Law, Effect of iron supply on Southern Ocean CO_2 uptake and implications for glacial atmospheric CO_2. *Nature* **407**, 730 (2000).
26. V. Brovkin, A. Ganopolski, D. Archer, S. Rahmstorf, Lowering of glacial atmospheric CO_2 is reponse to changes in oceanic circulation and marine biogeochemistry. *Paleoceanography* **22**, PA4202 (2007).
27. P. J. DiFiore *et al.*, Nitrogen isotope constraints on subantarctic biogeochemistry. *Journal of Geophysical Research* **11**, C08016 (2006).
28. N. Lang, E. W. Wolff, Interglacial and glacial variability from the last 800 ka in the marine, ice and terrestrial archives. *Climate of the Past* **7**, 361 (2011).
29. J. Russell, K. W. Dixon, A. Gnanadesikan, R. J. Stouffer, J. R. Toggweiler, The Southern Hemisphere Westerlies in a Warming World: Propping Open the Door to the Deep Ocean. *Journal of Climate* **19**, 6382 (2006).
30. A. M. de Boer, D. M. Sigman, J. R. Toggweiler, J. L. Russell, Effect of global ocean temperature change on deep ocean ventilation. *Paleoceanography* **22**, PA2210 (2007).
31. S. L. Jaccard, E. D. Galbraith, D. M. Sigman, G. H. Haug, A pervasive link between Antarctic ice core and subarctic Pacific sediment records over the past 800 kyrs. *Quaternary Science Reviews* **29**, 206 (2010).
32. B. Hönisch, N. G. Hemming, D. Archer, M. Siddall, J. McManus, Atmospheric Carbon Dioxide Concentration Across the Mid-Pleistocene Transition. *Science* **324**, 1551 (2009).
33. C. Le Quéré *et al.*, Trends in the sources and sinks of carbon dioxide. *Nature Geoscience* **2**, 831 (2009).

34. N. A. Rayner *et al.*, Global analyses of sea surface temperature, sea ice, and night marine air temperature since the late nineteenth century. *Journal of Geophysical Research* **108**, 4407 (2003).

35. B. Bereiter *et al.*, Mode change of millennial CO2 variability during the last glacial cycle associated with a bipolar marine carbon seesaw. *Proceedings of the National Academy of Sciences* **109**, 9755 (2012).

36. D. A. Hodell *et al.*, in *Proceedings of the Ocean Driling Program, Scientific Results,* R. Gersonde, D. A. Hodell, P. Blum, Eds. (Ocean Drilling Program, College Station, TX, 2003), vol. 177, pp. 1-26.

37. H. F. Kleiven, E. Jansen, in *Proceedings of the Ocean Drilling Program, Scientific Results,* R. Gersonde, D. A. Hodell, P. Blum, Eds. (Ocean Drilling Program, College station, TX, 2003), vol. 177, pp. 1-20.

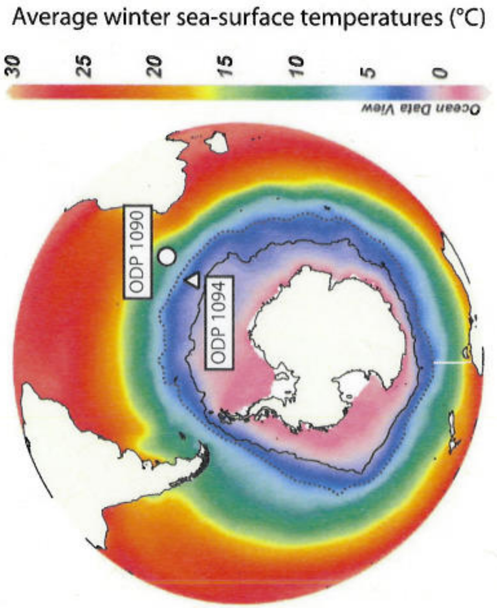
Average winter sea-surface temperatures (°C)
30
25
20
15
10
5
0
Ocean Data View
ODP 1090
ODP 1094

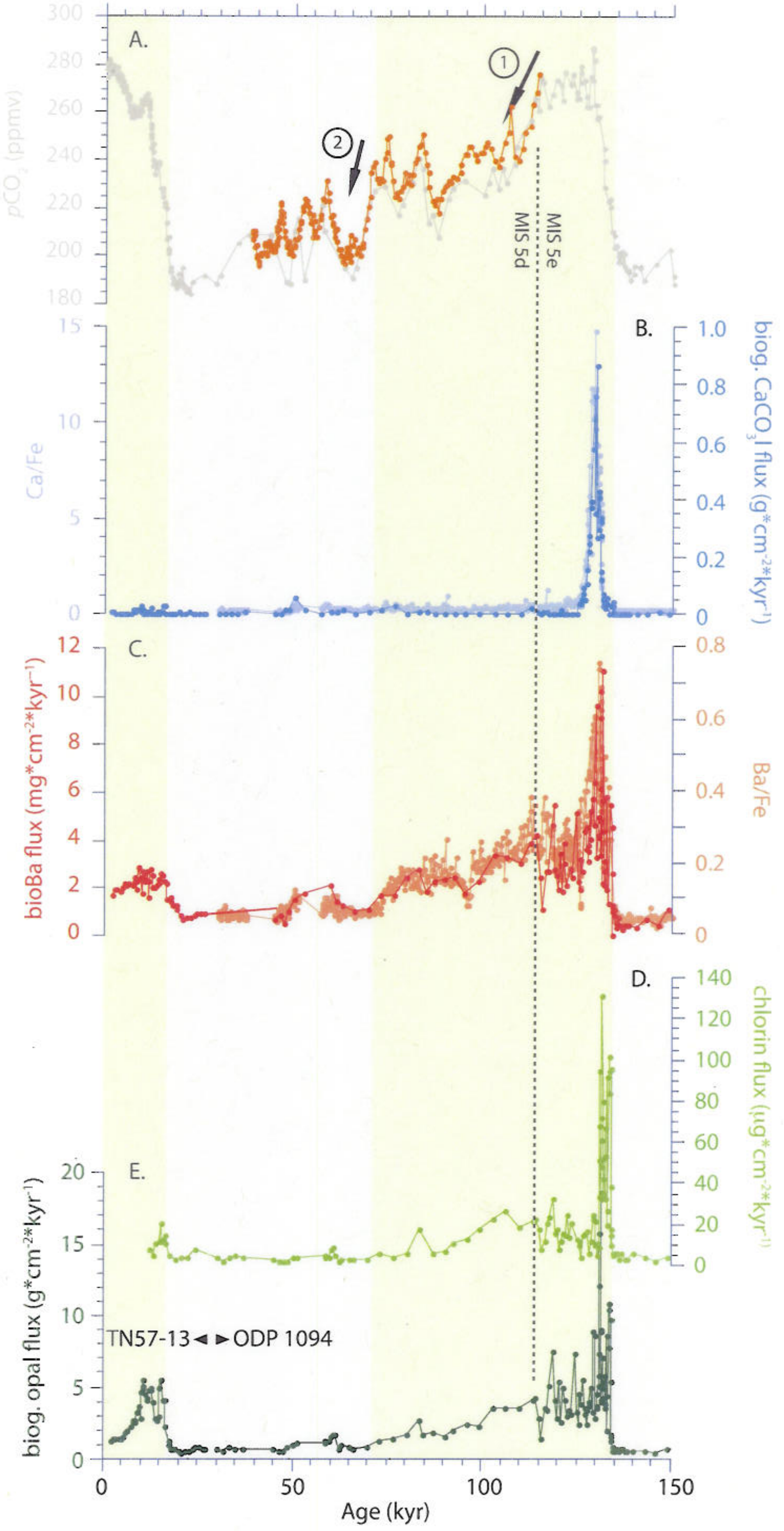
A.
pCO₂ (ppmv)
180
200
220
240
260
280
300
①
②
MIS 5d
MIS 5e
B.
Ca/Fe
0
5
10
15
biog. CaCO₃ flux (g*cm⁻²*kyr⁻¹)
0
0.2
0.4
0.6
0.8
1.0
C.
bioBa flux (mg*cm⁻²*kyr⁻¹)
0
2
4
6
8
10
12
Ba/Fe
0
0.2
0.4
0.6
0.8
D.
chlorin flux (µg*cm⁻²*kyr⁻¹)
0
20
40
60
80
100
120
140
E.
biog. opal flux (g*cm⁻²*kyr⁻¹)
0
5
10
15
20
TN57-13◄ ►ODP 1094
0
50
100
150
Age (kyr)

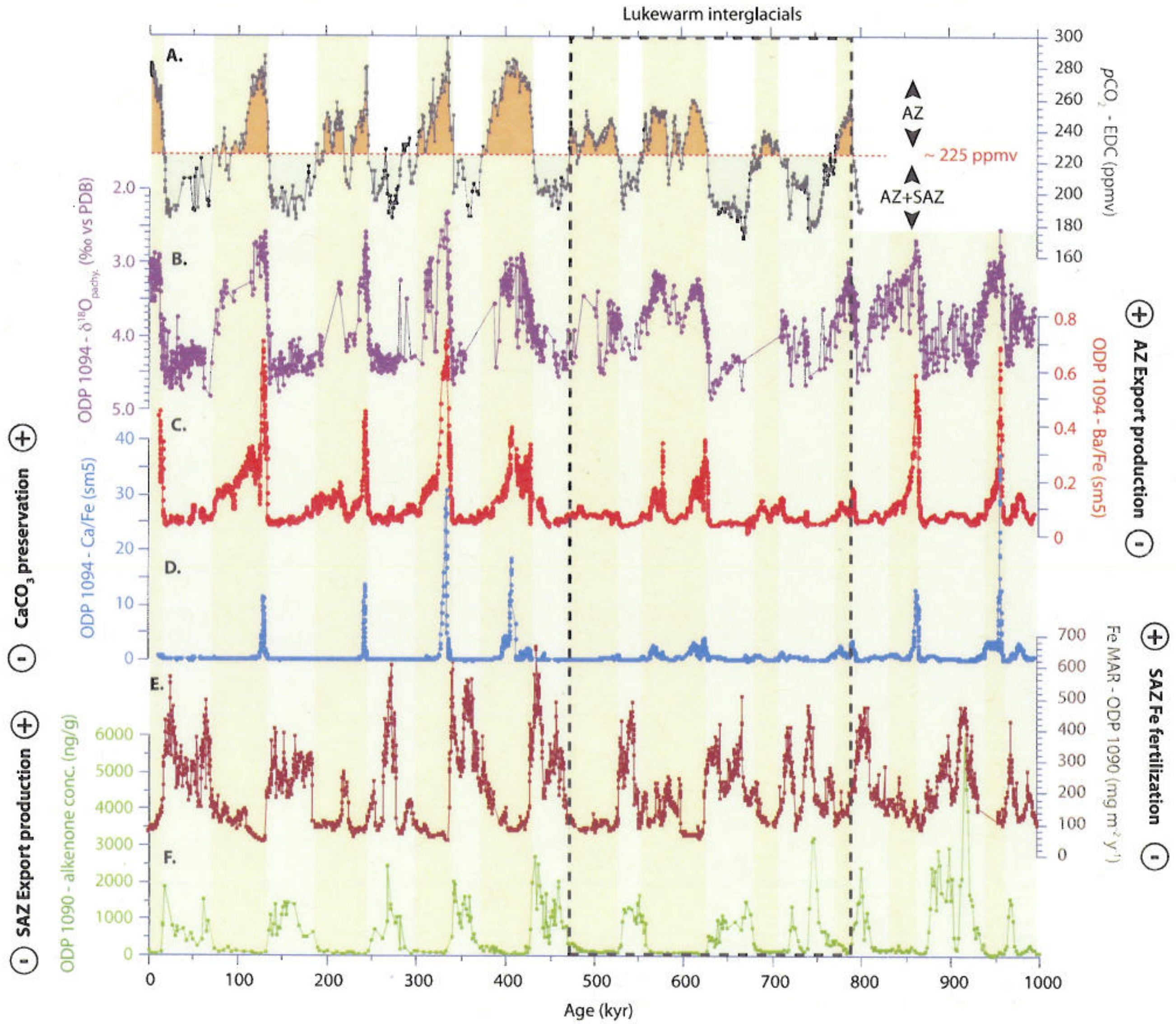
Lukewarm interglacials
A.
B.
C.
D.
E.
F.
AZ
~ 225 ppmv
AZ+SAZ
pCO$_2$ - EDC (ppmv)
300
280
260
240
220
200
180
160
ODP 1094 - δ^{18}O$_{pachy.}$ (‰ vs PDB)
2.0
3.0
4.0
5.0
ODP 1094 - Ba/Fe (sm5)
0.8
0.6
0.4
0.2
0
AZ Export production
ODP 1094 - Ca/Fe (sm5)
40
30
20
10
0
CaCO$_3$ preservation
Fe MAR - ODP 1090 (mg m^{-2} y^{-1})
700
600
500
400
300
200
100
0
SAZ Fe fertilization
ODP 1090 - alkenone conc. (ng/g)
6000
5000
4000
3000
2000
1000
0
SAZ Export production
0
100
200
300
400
500
600
700
800
900
1000
Age (kyr)

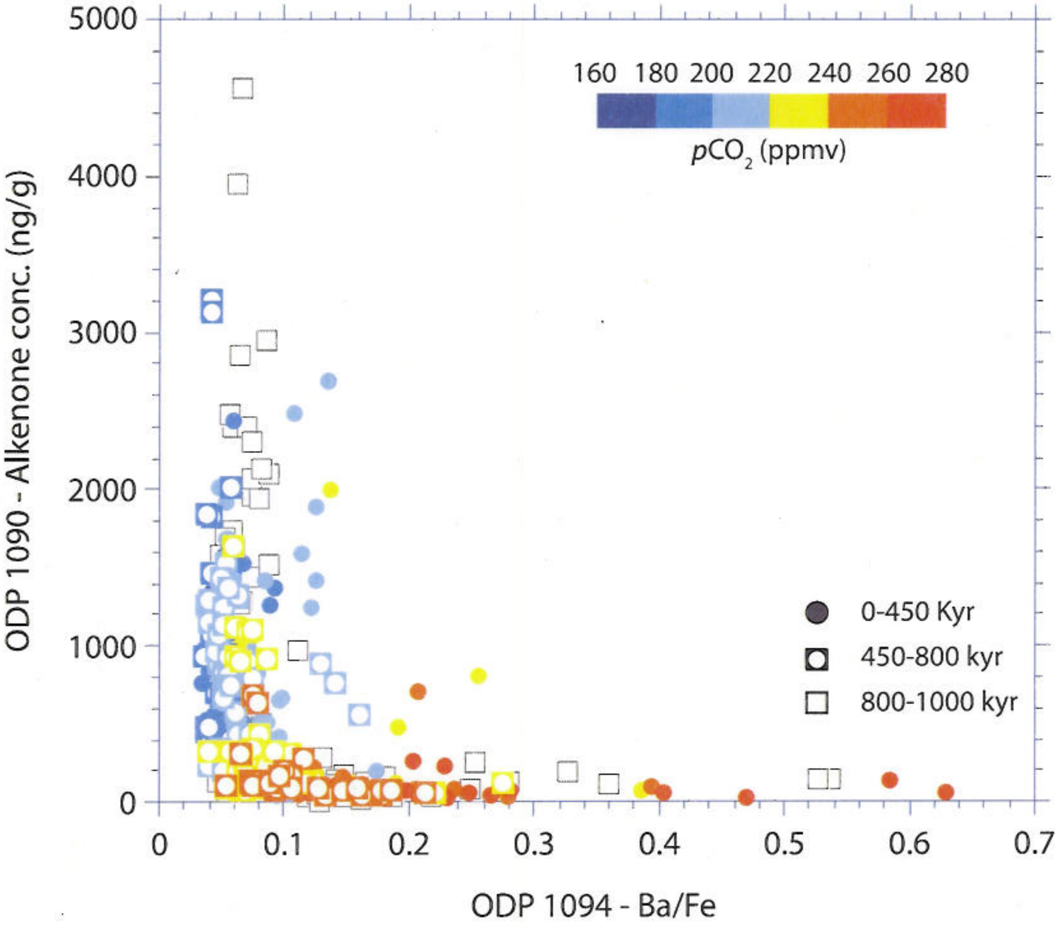

160 180 200 220 240 260 280
pCO$_2$ (ppmv)
● 0-450 Kyr
○ 450-800 kyr
☐ 800-1000 kyr
ODP 1090 - Alkenone conc. (ng/g)
5000
4000
3000
2000
1000
0
0
0.1
0.2
0.3
0.4
0.5
0.6
0.7
ODP 1094 - Ba/Fe